Three-body unitarity, the cloudy bag model, and the Roper resonance

B. C. Pearce*
Theoretical Division, Los Alamos National Laboratory, Los Alamos, New Mexico 87545

I. R. Afnan
School of Physical Sciences, The Flinders University of South Australia, Bedford Park, South Australia 5042, Australia
(Received 26 October 1988)

We present the details and results of a Faddeev calculation of πN scattering in the P_{11} channel in the region of the Roper resonance. Our equations respect two- and three-body unitarity, treat the nucleon and delta on an equal footing, and have a pole with correct residue at the nucleon mass. The input is from the cloudy bag model. Resonance behavior is exhibited without the inclusion of a bare Roper bag, although not in detailed agreement with experiment. If a bare Roper bag is included, the phase shifts vary far too rapidly in the resonance region, implying that identifying the lowest radial bag excitations with the Roper leads to a physical Roper that is much too narrow.

I. INTRODUCTION

The πN system has recently become the subject of renewed interest. There are three notable reasons for this interest. First is the need for reliable amplitudes to be used as input to π-nucleus calculations. This is becoming increasingly important as higher energy pion beams become available and the details of the πN interaction beyond the delta resonance are probed. Second, the πN system is a nice testing ground for QCD motivated hadron models. Finally, and closely related to both preceding points, there is the question of the nature of some of the πN resonances. On the one hand we have models that attempt to describe these resonances as various excitations of three-quark states,[1-4] while others have pointed out that they may be due to the opening of inelastic thresholds.[5,6]

Considerable effort has been expended on various quark models of hadrons. An example is the nonrelativistic quark potential model[1] and, more recently, the relativized quark potential model.[2] In these models, a confining potential for the quarks is postulated, the resulting Lagrangian diagonalized in some basis, and the resulting eigenenergies compared with the experimental hadron spectrum. At a later point,[3] the decay modes of the states are investigated by computing matrix elements of some Lagrangian describing the decay vertex between states obtained via the initial procedure. This points to a serious flaw in these models; namely, that pionic self-energy graphs are not included when computing the mass spectrum of the baryons. These terms will have a significant contribution not only to the widths but also the positions of the predicted masses. The situation is even worse when one considers the excited states that have substantial widths, often with substantial partial widths for decay to two pion states. The lowest in energy of these states is the Roper or $N^*(1440)$. The data tables[7] list its mass at 1400–1480 MeV with a full width of 120–350 MeV. It decays 30–50 % of the time to $\pi\pi N$, the rest being to πN. Of the $\pi\pi N$ contribution, 10–20 % is via $\pi\Delta$, 10–15 % is via ρN, and 5–20 % is $N(\pi\pi)_S$ where $(\pi\pi)_S$ is the strong isospin 0, S-wave $\pi\pi$ interaction. Clearly from these observations, the state listed in the data tables as the Roper has been extracted from an energy dependent background dominated by the $\pi\pi N$, $\pi\Delta$, ρN, and $N(\pi\pi)_S$ thresholds. This means that a model that purports to predict the masses of such states should include this energy dependent background. In particular, this means that such a model should include the coupling of the baryons to the pion cloud.

The cloudy bag model[8-11] provides a reasonable starting point in this regard. Here the coupling to the pions enters naturally by restoring chiral symmetry to the MIT bag. Since this provides a description of the pion-baryon interaction we are now able to examine the scattering. In this way we can ensure that the energy dependent background, and in particular the various thresholds, can be included in a natural way. Using an $SU(3)$ extension of the cloudy bag model that couples kaons to the baryons, it has been shown[12] that the $\Lambda^*(1405)$ emerges as a $\bar{K}N$ bound state, rather than a quark state. Similarly, in the cloudy bag model the Δ is predominantly a three-quark state[8] as opposed to the πN resonance state of the Chew-Low picture.[13] Although the cloudy bag model bears some similarity to the old Chew-Low model, it differs in one important respect, as a consequence of its consistency with QCD. That is, the nucleon and delta are treated on an equal footing. Also, the bare πNN, $\pi N\Delta$, and $\pi\Delta\Delta$ coupling constants are all related.

There have been several treatments of πN scattering based on the cloudy bag model. The first calculations[8] obtained good results for the P_{33} channel by iterating the delta pole and crossed diagrams in a Lippmann-Schwinger equation. Later, Rinat[14] calculated scattering in the P_{11} channel using iterations of just the nucleon and Roper pole diagrams (treating the bare Roper as the lowest radial excitation of the nucleon). In that calculation, the Roper pole provides the only attraction and it was necessary to adjust the Roper radius separately from that of the nucleon in order to obtain reasonable agree-

ment with experiment. The calculation of Suzuki *et al.* achieves surprisingly good results for $T_\pi < 500$ MeV by uniterizing the pole and crossed diagrams in a Heitler equation. Although they conjecture that the contributions from multiple scattering are negligible, our experience[15] is that this is not so.

All of these early cloudy bag model calculations use the version where the pions couple to the quarks only at the bag surface and therefore do not incorporate the contact diagram that arises when the pions are allowed to couple throughout the bag volume. The contact diagram allowed calculations of S-wave scattering which were not possible in the original form. Cooper and Jennings[16] have shown that the low energy S waves can be well reproduced. The first attempt to include the contact diagram in the P_{11} channel[9] did not succeed in reproducing the low energy experimental phase shifts. However, in an earlier paper,[15] we demonstrated that this problem is cured by ensuring that the P_{11} amplitude has a pole with correct residue at the nucleon mass. The success of the cloudy bag model for low energy scattering suggests that it should form a good basis for calculations above the pion production threshold.

Having chosen a Lagrangian to work with, we now need to find a scheme for calculating unitary scattering amplitudes. Here we are confronted with two problems. Firstly, the P_{11} channel contains the nucleon pole. This means that our scattering amplitude must have a pole at the physical nucleon mass with the appropriate residue. Secondly, since the Roper resonance occurs above the pion production threshold, our amplitudes should be consistent with two- and three-body unitarity. In summary then, what we seek is a solution that treats the nucleon and delta on an equal footing, has a pole with correct residue at the nucleon mass, and satisfies two- and three-body unitarity. Such a scheme has not been attempted before. Recent calculations using the cloudy bag model[9,15] use the Lippmann-Schwinger equation which only satisfies two-body unitarity and is therefore inappropriate in the vicinity of the Roper resonance.

In order to develop a suitable framework for a calculation of πN scattering that includes a correct description of the inelastic thresholds, we presented in Ref. 17 a formal derivation of a set of three-body equations for the πN-$\pi\pi N$ system. The derivation utilized the technique of classification of diagrams according to their reducibility that has been used successfully in the πNN system.[18–20] As a guide to the classification process, we consider the basic interactions to be governed by the cloudy bag model.[8] The resulting coupled integral equations sum the subset of all diagrams (generated from the $B \to \pi B$ vertex and $\pi B \to \pi B$ contact diagrams) that are needed to ensure two- and three-body unitarity. We note that a similar set of equations for the πN-$\pi\pi N$ system has been derived using projection operator techniques by Fuda.[21] However, his equations admit only the $B \to \pi B$ vertex as the basic interaction. Also we note that there has been no attempt to perform a numerical calculation based on these equations.

To the best of our knowledge, there have been two other calculations of the πN system within the framework of a set of integral equations that respect two- and three-body unitarity. The first is due to Aaron, Amado, and Young[5] in the late 1960s. They find that Δ and ρ production are important mechanisms in the D_{13}, D_{33}, and P_{13} channels. However, they do not perform a detailed calculation of the P_{11} channel. Also, in the light of modern bag models, their theory is inadequate in the sense that it does not treat the nucleon and delta on an equal footing. More recently, Garcilazo and Mathelitsch[22] have performed a very similar calculation to Aaron, Amado, and Young. Again, their calculation does not treat the nucleon and delta on an equal footing. They generally arrive at similar conclusions; namely, that some of the πN resonances may be caused by threshold effects. However, the agreement with experiment is again only qualitative. Particularly, the agreement in the P_{11} channel to a pion lab energy of about 900 MeV is very poor.

The three-body equations presented in Ref. 17 have an important consequence for low energy scattering when three-body unitarity can be neglected. That is, the vertices forming the crossed diagram are dressed and should reproduce the physical coupling constant. However, most two-body calculations that consider this diagram[8,9] have the bare coupling constant in the crossed diagram as well as the pole diagram. Putting this into practice in Ref. 15, we found that we were able to reproduce the low energy P_{11} phase shifts quite well. We also determined the bare coupling constant needed to reproduce the experimental value by evaluating the same series of diagrams that are summed by the scattering equations. Using this procedure we found that we needed a much smaller value of the bare coupling constant than found by previous authors[8] who evaluate only the lowest order contributions.

From the derivation of the equations given in Ref. 17, it is clear that the input is the solution to the same set of equations but at lower energy. (At such energies, it should be possible to neglect most of the contribution to three-body unitarity as was done in Ref. 15.) However, in order to achieve equations that are practical from a computational point of view, we require that the input πN and $\pi\pi$ interactions be described by separable potentials. Unfortunately, neither the crossed diagram nor the contact diagram which form the input to the equation is separable. In the P_{11} channel, these two diagrams provide the attraction required to cancel the repulsive nucleon pole and hence should be treated with care.

To overcome this dilemma, we need to find a suitable approximation to the combined crossed and contact diagrams that is separable. If we are to not depart too far from our goal of summing all diagrams from the Lagrangian consistent with two- and three-body unitarity, we must ensure that the approximation we choose is consistent with the calculation of Ref. 15. The way we choose to do this is by making a separable expansion of the combined crossed and contact diagrams using an energy dependent extension[23] of the standard EST (Ernst, Shakin, and Thaler[24]) method.

In this paper we present the details and results of a full three-body calculation of the πN system, which includes coupling to the $\pi\Delta$ and ρN channels. We begin in Sec. II

with a brief review of the equations derived in Ref. 17. To perform calculations with these equations they must be cast in a form suitable for numerical solution. The steps involved are to rewrite the equations for the case of separable input, symmetrize with respect to the two pions, and perform a partial wave expansion. These steps are similar to the corresponding steps needed to produce numerical results for the πNN system.[25,18] However, the symmetrization involves some subtleties not present in the πNN system (due mainly to the fact that the particles we are symmetrizing can be created and destroyed) so we include the details of the symmetrization in the Appendix.

In Sec. III we provide a full description of the two-body input used in the calculation. The derivation of the equations clearly indicates that the input should be the solution to the same equations but at lower energy. However, to keep the calculation manageable, we require that the input be separable. In Sec. III we show how the separable expansion method of Ref. 23 is used to resolve this.

The renormalization procedure employed to ensure that the P_{11} amplitude has a pole with correct residue at the nucleon mass is presented in Sec. IV. In particular, we show how the renormalization of the input two-body amplitude effects the renormalization of the three-body equations.

The results are presented in Sec. V. Most notably, we find that resonance behavior that is nearly in accord with experiment is possible without the inclusion of a (radially excited) bare Roper bag, while inclusion of such a state leads to a dressed Roper that is much too narrow. Our concluding remarks are presented in Sec. VI.

II. SUMMARY OF EQUATIONS

In Ref. 17 we presented a set of equations for the πB-$\pi\pi B$ system that respect two- and three-body unitarity and treat the nucleon and delta on an equal footing. For completeness and to establish the notation, we begin by presenting a summary of these equations.

The equations of Ref. 17 are derived by considering classes of diagrams of a given reducibility. By explicitly exposing all diagrams with n-particle intermediate states, a set of equations can be derived that satisfy n-body unitarity. The first step in deriving equations satisfying three-body unitarity is to derive the two-body equations. As described in Ref. 17, the total $\pi B \to \pi B$ amplitude $T_{BB}^{(0)}$ is

$$T_{BB}^{(0)} = T_{BB}^{(1)} + f^{(1)\dagger} d f^{(1)} . \tag{2.1}$$

Here $f^{(1)}$ is the one-particle irreducible $B \to \pi B$ vertex function and d is the dressed baryon propagator. The parenthesized superscript specifies the irreducibility of the amplitude.

Since we take the πB space to include πN and $\pi\Delta$, T_{BB} is a 2×2 matrix. The rank of the $B \to \pi B$ vertex matrix f depends on how many baryons are included in the B space. For example, if we include N, Δ, and Roper, then f is a 3×2 matrix. In this case d will be a 3×3 matrix.

The dressed vertex function $f^{(1)}$ is given by

$$f^{(1)} = f^{(2)} + f^{(2)} g T_{BB}^{(1)} , \tag{2.2}$$

and the baryon propagator is

$$d = (d_0^{-1} - \Sigma^{(1)})^{-1} , \tag{2.3}$$

where the one-particle irreducible self-energy $\Sigma^{(1)}$ is

$$\Sigma^{(1)} = \Sigma^{(2)} + f^{(2)} g f^{(1)\dagger} . \tag{2.4}$$

Also, d_0 is the bare baryon propagator. This is a diagonal matrix with elements given by

$$d_{0\alpha}(E) = (E - m_{0\alpha})^{-1} , \tag{2.5}$$

where α can be any of the baryons in the single baryon space. We variously take this space to include just the nucleon and delta or the nucleon, delta, and Roper. However, we always restrict the baryon in the pion plus baryon space to the nucleon and delta. In these equations, g is the πB propagator. The driving term for the vertex and propagator dressing is the one-particle irreducible amplitude $T_{BB}^{(1)}$ which is given by

$$T_{BB}^{(1)} = T_{BB}^{(2)} + T_{BB}^{(2)} g T_{BB}^{(1)} . \tag{2.6}$$

Since we have now exposed all two-particle intermediate states, Eqs. (2.1)–(2.6) describe the πB scattering process in a manner consistent with two-body unitarity. By taking the two-particle irreducible amplitudes from the cloudy bag model we have the set of equations that was examined in Ref. 15. To obtain three-body unitarity we must continue until all three-body states have been exposed.

As discussed in Ref. 17, in carrying out this procedure we are forced to neglect the contribution from the $B \to \pi\pi B$ vertex. This appears in the cloudy bag model Lagrangian as a different time ordering of the contact diagram. Including diagrams of this type increases the complexity of the resulting equations to the point where it becomes difficult to find a convenient closed form for the quasi-two-body scattering amplitudes. As pointed out,[17] it is possible to include the lowest order contributions of this vertex perturbatively. We do not attempt this at this stage.

By neglecting contributions from $B \to \pi\pi B$ vertices, Eq. (2.6) becomes

$$T_{BB}^{(1)} = \left[T_{BB}^{(3)} + \sum_{i,j} F_d^{(2)}(i) \bar{\delta}_{ij} G F_d^{(2)\dagger}(j) \right] \times (1 + g T_{BB}^{(1)}) + \sum_{i,\lambda} F_d^{(2)}(i) G \bar{\delta}_{i\lambda} M_d^{(2)}(\lambda) G T_{\lambda B}^{(1)} , \tag{2.7}$$

with

$$T_{\lambda B}^{(1)} = \sum_i \bar{\delta}_{\lambda i} F_d^{(2)\dagger}(i)(1 + g T_{BB}^{(1)}) + \sum_\alpha \bar{\delta}_{\lambda\alpha} M_d^{(2)}(\alpha) G T_{\alpha B}^{(1)} . \tag{2.8}$$

Here the indices i and j run over the two pions (labeled 1 and 2) while λ and α run over the pions and the baryon (the baryon is particle 3). The amplitude $T_{\alpha B}^{(1)}$ is the one-particle irreducible amplitude for scattering from a state

which is a bound or resonant state of two particles with the third one spectating. We depart from usual spectator notation in that for $\lambda=1,2$, λ specifies the interacting pion while $\lambda=3$ represents the case of a $\pi\pi$ interaction with a baryon spectator. The amplitude $F_d^{(2)}(i)$ is the disconnected $\pi B \to \pi\pi B$ amplitude in which pion i interacts with the baryon. It is given by

$$F_d^{(2)}(i)=\sum_j \bar{\delta}_{ij} d_\pi^{-1}(j) f^{(1)}(i) , \tag{2.9}$$

where $d_\pi(j)$ is the propagator of pion j. This amplitude is illustrated in Fig. 1. Also in Eqs. (2.7) and (2.8) we have the disconnected $\pi\pi B \to \pi\pi B$ amplitude $M_d^{(2)}(\alpha)$ given by

$$M_d^{(2)}(i)=\sum_j \bar{\delta}_{ij} d_\pi^{-1}(j) T_{BB}^{(1)}(i) , \tag{2.10}$$

and

$$M_d^{(2)}(3)=d^{-1} T^{(1)}(3) . \tag{2.11}$$

Here, $T^{(1)}(3)$ is the $\pi\pi$ amplitude which we assume satisfies an equation of the form

$$T^{(1)}(3)=T^{(2)}(3)+T^{(2)}(3) d_\pi d_\pi T^{(1)}(3) , \tag{2.12}$$

where $T^{(2)}(3)$ is the $\pi\pi$ potential. The amplitude $M_d^{(2)}(\alpha)$ is illustrated in Fig. 2. Finally, we note that G is the free three-particle propagator.

As noted in Ref. 17, to solve for the full πB amplitude we can either solve Eqs. (2.7) and (2.8) for $T_{BB}^{(1)}$ and then use Eqs. (2.1)–(2.4) to obtain $T_{BB}^{(0)}$ or we can solve directly for $T_{BB}^{(0)}$ by solving the system of equations

$$T_{BB}^{(0)}=V_{BB}(1+gT_{BB}^{(0)})+\sum_{i,\lambda} F_d^{(2)}(i) G \bar{\delta}_{i\lambda} M_d^{(2)}(\lambda) G T_{\lambda B}^{(0)} , \tag{2.13}$$

and

$$T_{\lambda B}^{(0)}=\sum_i \bar{\delta}_{\lambda i} F_d^{(2)\dagger}(i)(1+gT_{BB}^{(0)})+\sum_\alpha \bar{\delta}_{\lambda\alpha} M_d^{(2)}(\alpha) G T_{\alpha B}^{(0)} , \tag{2.14}$$

with

$$V_{BB}=f^{(2)\dagger} d_0 f^{(2)}+T_{BB}^{(3)}+\sum_{i,j} F_d^{(2)}(i) G \bar{\delta}_{ij} F_d^{(2)\dagger}(j) . \tag{2.15}$$

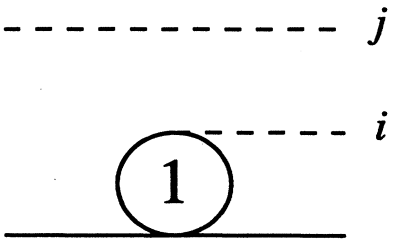

FIG. 1. The disconnected $\pi B \to \pi\pi B$ amplitude, $F_d^{(2)}(i)$.

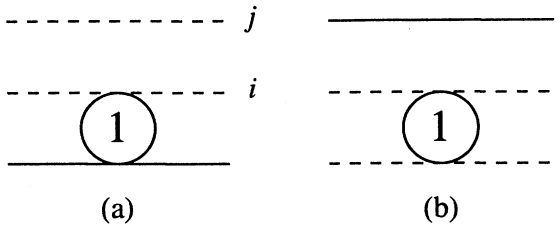

FIG. 2. The disconnected $\pi\pi B \to \pi\pi B$ amplitudes: (a) $M_d^{(2)}(i)$ and (b) $M_d^{(2)}(3)$.

The latter approach has the advantage of not requiring the solution to the integral equations [Eqs. (2.7) and (2.8)] for the fully off-shell amplitudes.

The coupled equations for the πB-$\pi\pi B$ system that we proceed to solve in the following sections are given by Eqs. (2.13)–(2.15).

III. TWO-BODY INPUT

In order to perform calculations using the equations summarized in Sec. II we must perform two major operations. First, we must write the equations for the case of separable two-body input interactions. In the same step, we symmetrize the equations with respect to the two pions. This is necessary since in the original derivation the pions were regarded as distinguishable. We have presented this derivation in the Appendix. The second task is to expand the matrix nature of the equations and

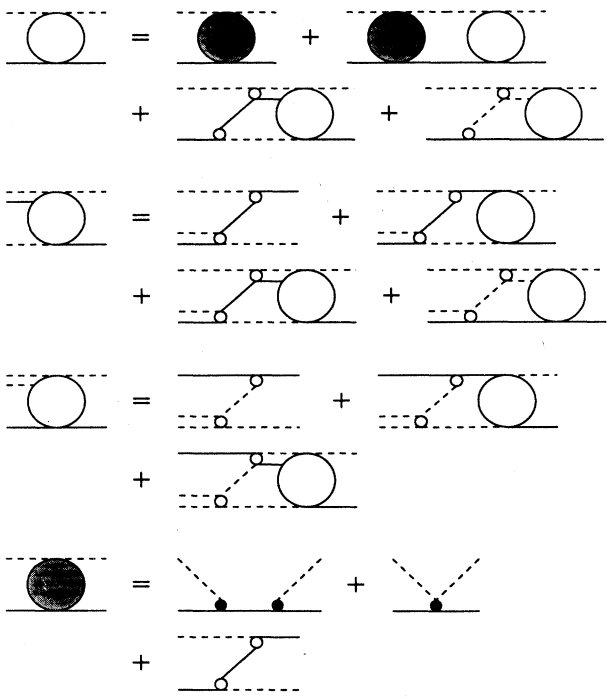

FIG. 3. The graphical equivalent of Eqs. (A6) and (A7).

perform a partial wave expansion. Since this is done in a similar way to the πNN system we refer the interested reader to Refs. 25 and 26.

The integral equations that we obtain are given in Eqs. (A6) and (A7). They are depicted graphically in Fig. 3. These equations include coupling of πB states (where the B is dressed by the two-body input πB interaction) to states where one pion interacts with the baryon while the other spectates (denoted πB^*), and states where the two pions interact and the baryon spectates (denoted ρB). The driving terms of the integral equations are the baryon and pion exchange terms shown graphically in Figs. 4 and 5. Their derivation[26] is similar to that for other three-body systems.[18]

We have now only to specify the two-body input to our equations in order to complete the description of the calculation. The two-body input enters through the πB, πB^*, and $B\rho$ propagators τ_B, τ_{B^*}, and τ_ρ as well as through the one-particle irreducible πBB vertex function $f^{(1)}$. The derivation of the equations that we have presented clearly indicates that the input arises as the lower energy solution of the same equations such as that presented in Ref. 15. However, the practical necessity to use separable input means we need to find separable approximations to the nonpole potentials used in Ref. 15. Since the crossed diagram is energy dependent we use the modification of the Ernst, Shakin, and Thaler scheme[24] described in Ref. 23. Such a scheme allows a rank N approximation to the potential, that ensures the resulting t matrix is exact at N selected energies.

We are now confronted with a small notational problem. We need to distinguish between the amplitudes that are solutions of the full three-body equations and those that are the approximate solution of the two-body equations that are used as input to the three-body calculation. The convention we use is to place a bar over quantities that are solutions of the two-body equations. Hence, T_{BB} becomes $\bar{T}$, etc. (the BB subscript is unnecessary for the two-body amplitudes since there is no coupling to πB^* or ρB states).

By a slight generalization of the expansion method of Ref. 23, it is possible to ensure that the separable expansion for the P_{11} channel preserves the renormalization results of Ref. 15, i.e., the πNN coupling constant does not

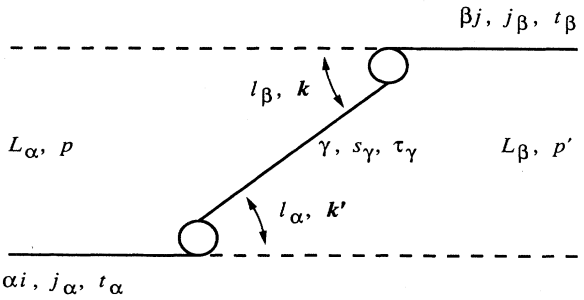

FIG. 4. The baryon exchange diagram, $Z^{JT}_{\alpha i;\beta j}(p,p';E)$.

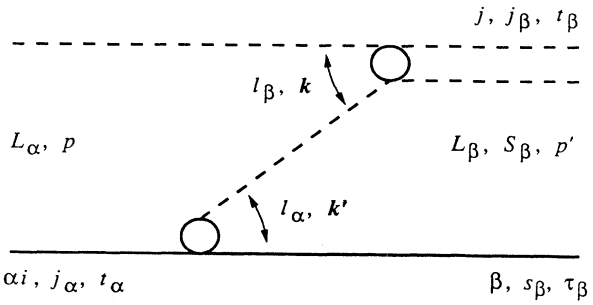

FIG. 5. The π exchange diagrams, $Z^{JT}_{\alpha i;\rho\beta j}(p,p';E)$.

change upon the replacement of $\bar{T}^{(2)}$ by a separable expansion. We take our (partial wave expanded) separable potential to be of the form

$$\bar{T}^{(2)}_S(E)=\sum_{i,j=1}^{N}\bar{T}^{(2)}(E_i)|u_i\rangle\lambda_{ij}(E)\langle u_j|\bar{T}^{(2)}(E_j)\rangle\ . \tag{3.1}$$

To maintain the energy dependence of the original potential, $\bar{T}^{(2)}(E)$, we take for the strength $\lambda_{ij}(E)$, the solution of the equation

$$\langle u_m|\bar{T}^{(2)}(E)|u_n\rangle=\sum_{i,j=1}^{N}\langle u_m|\bar{T}^{(2)}(E_i)|u_i\rangle \times\lambda_{ij}(E)\langle u_j|\bar{T}^{(2)}(E_j)|u_n\rangle\ . \tag{3.2}$$

In the case we are considering here we note that $|u_i\rangle$ must be a 2×1 matrix to account for the coupled πN and $\pi\Delta$ channels. To guarantee that the separable expansion $\bar{T}^{(2)}_S(E)$ gives the same half-off-shell T matrix as the original potential $\bar{T}^{(2)}(E)$ at selected energies E_i, we need to choose the functions $|u_i\rangle$ to be the scattering wave function for the potential $\bar{T}^{(2)}(E)$ at the energies E_i. In this case the form factors of the separable approximation are

$$\begin{aligned}\bar{T}^{(2)}(E_i)|u_i\rangle&=\bar{T}^{(2)}(E_i)|\psi_{E_i,\alpha_i}\rangle\\&=\bar{T}^{(1)}(E_i)|k_i\alpha_i\rangle\ .\end{aligned} \tag{3.3}$$

Although the above procedure guarantees the half-off-shell amplitude to be exact at select energies, there is no such guarantee for the full-off-shell amplitude. As a result, the separable expansion is not guaranteed to give the renormalization in Ref. 15, and in particular, it does not preserve the value of the πNN coupling constant. This results from the term $\bar{T}^{(1)}(m_N)g(m_N)\bar{f}^{(2)\dagger}|N\rangle$ in the expression for $\bar{f}^{(1)\dagger}(m_N)|N\rangle$ as given in Eq. (2.2). Here, we observe that

$$\begin{aligned}\bar{T}^{(1)}g\bar{f}^{(2)\dagger}&=(\bar{T}^{(2)}+\bar{T}^{(2)}g\bar{T}^{(1)})g\bar{f}^{(2)\dagger}\\&=\bar{T}^{(2)}g(\bar{f}^{(2)\dagger}+\bar{T}^{(1)}g\bar{f}^{(2)\dagger})\\&=\bar{T}^{(2)}g\bar{f}^{(1)\dagger}\ .\end{aligned} \tag{3.4}$$

Hence by choosing one of the $|u_i\rangle$'s to be given as

$$|u_i\rangle=g(m_N)\bar{f}^{(1)\dagger}(m_N)|N\rangle\ , \tag{3.5}$$

TABLE I. Form factor parameters for πN input [see Eq. (3.7)].

$ljt(i)$	μ	$n_{Ni\mu}$	$m_{Ni\mu}$	$c_{Ni\mu}$ (fm$^{n+1/2}$)	$\beta_{Ni\mu}$ (fm^{-1})	$n_{\Delta i\mu}$	$m_{\Delta i\mu}$	$c_{\Delta i\mu}$ (fm$^{n+1/2}$)	$\beta_{\Delta i\mu}$ (fm^{-1})
$P_{11}(1)$	1	1	2	0.1942	2.626	1	2	0.2199	3.006
	2	3	5	0.0235	5.260	3	5	0.0255	5.706
	3	5	50	-0.413×10^{-4}	31.22	5	50	-0.644×10^{-4}	31.72
$P_{11}(2)$	1	1	2	−0.3453	2.619	1	2	−0.4044	2.271
	2	3	5	−0.0303	5.407	3	5	−0.0372	5.115
	3	5	50	0.984×10^{-4}	30.02	5	50	0.512×10^{-4}	31.50
	4	7	50	−0.3044	2.704	7	50	−0.3044	2.704
$P_{33}(1)$	1	1	2	−0.1137	1.497	1	2	−0.1333	1.911
	2	3	5	−0.0192	3.345	3	5	−0.0157	4.438
	3	5	50	0.810×10^{-5}	21.79	5	50	0.825×10^{-5}	32.49

we are guaranteed that

$$\bar{T}_S^{(2)}(m_N)|u_i\rangle=\bar{T}^{(2)}(m_N)|u_i\rangle$$
$$=\bar{T}^{(2)}(m_N)g(m_N)\bar{f}^{(1)\dagger}(m_N)|N\rangle\ . \quad (3.6)$$

In this way $\bar{f}^{(1)\dagger}(m_N)|N\rangle$ retains its value when $\bar{T}^{(2)}(E)$ is replaced by the separable approximation $\bar{T}_S^{(2)}(E)$.

In practice we implement the above prescription by calculating the form factors and λ functions and then fitting them with suitable functions. To be precise, we fit the form factors $\langle p,\pi\alpha|\bar{T}^{(2)ljt}(E_i)|u_i\rangle$ $(\alpha=N,\Delta)$ with functions $\phi_i^{ljt}(\alpha;p)$ of the form

$$\phi_i^{ljt}(\alpha;p)=\sum_{\mu=1}^{M_\sigma}\frac{c_{\sigma,\mu}p^{n_{\sigma,\mu}}}{(1+p^2/\beta_{\sigma,\mu}^2)^{m_{\sigma,\mu}}}\ , \quad (3.7)$$

where σ stands for the labels ljt, i, and α (ljt specifies the partial wave). The functions $\lambda_{ij}(E)$ are fitted by $\Lambda_{ij}^{ljt}(E)$ where

$$\Lambda_{ij}^{ljt}(E)=\frac{A_{ij}^{ljt}}{E-B_{ij}^{ljt}}+\frac{C_{ij}^{ljt}}{E-D_{ij}^{ljt}}+E_{ij}^{ljt}\ . \quad (3.8)$$

The parameters for these functions are given in Tables I and II. We use a rank 2 approximation to the P_{11} input and rank 1 for the P_{33}. We stress that these parameters are not fitted to experimental data but to the functions resulting from performing the expansion described above.

To summarize, the total potential in partial wave γ is then[15]

$$\bar{V}_{\alpha\beta}^{\gamma}(p,p';E)=\bar{T}_{\alpha\beta}^{(2)\gamma}(p,p';E)+\frac{\bar{f}_{\pi\alpha\gamma}^{(2)}(p)\bar{f}_{\gamma\beta\pi}^{(2)}(p')}{E-\bar{m}_{0\gamma}}\ , \quad (3.9)$$

where

$$\bar{T}_{\alpha\beta}^{(2)\gamma}(p,p';E)=\sum_{i,j}\phi_i^{\gamma}(\alpha,p)\Lambda_{ij}^{\gamma}(E)\phi_j^{\gamma}(\beta,p')\ . \quad (3.10)$$

The subscripts i and j run over the (arbitrary) rank of the separable expansion. We have shown explicitly the matrix nature of the potential using the labels α and β. The label γ is used both to specify the partial wave and the corresponding baryon. In partial waves other than the P_{11} and P_{33} this reduces to just the nonpole part, $\bar{T}^{(2)}$. In this calculation, however, we have not included any πN channels other than the P_{11} and P_{33}. The scattering amplitude $\bar{T}^{(0)}$ can now be calculated by iterating this two-term, separable potential in a Lippmann-Schwinger equation. Similarly, the nonpole part of the amplitude, $\bar{T}^{(1)}$, that is used to determine the dressing of the vertices in the crossed diagram is obtained by solving the two-body equations [Eq. (2.6)] for the potential, $\bar{T}^{(2)}$.

The separable approximation to the nonpole potential $\bar{T}^{(2)}(E)$ obtained in this way reproduces very well the on-shell nonpole and total amplitudes obtained in Ref. 15. However, as noted in Ref. 15, the width is too narrow in the P_{33} channel. Hence, rather than propagate this error in the form of a $\pi\Delta$ threshold that is too close to the real axis, we choose to use a larger bare coupling constant in the P_{33} input than that necessary to correctly reproduce the nucleon pole in the P_{11} channel. In the P_{11} channel we use $\bar{f}_0=0.031\,96$ and $\bar{m}_{0N}=1086$ MeV while in the P_{33} channel we have $\bar{f}_0=0.07$ and $\bar{m}_{0\Delta}=1475$ MeV. The results of this expansion procedure are illustrated in Figs. 6 and 7. Figure 6 shows the P_{11} phase shifts while Fig. 7 is the P_{33}. In both cases, (a) are the total phase shifts, the data being from the

TABLE II. $\Lambda(E)$ parameters for πN input [see Eq. (3.8)].

ljt	i	j	A_{ij}	B_{ij} (MeV)	C_{ij}	D_{ij} (MeV)	E_{ij}
P_{11}	1	1	−17.33	2660	2.179	1502	−11.82
	1	2	−10.71	2670	2.287	1504	−7.565
	2	2	−5.769	2798	2.428	1515	−5.292
P_{33}	1	1	17.41	1744	0		−3.112

Karlsruhe-Helsinki phase shift analysis,[27] while (b) are the nonpole phase shifts with the solid curves showing the results of the separable expansion and the dashed curves showing the results of Ref. 15. The small difference in the nonpole amplitudes is a reflection on the quality of fit for the on-shell phases of our expansion, while the total phases give an indication as to the accuracy of the expansion for the off-shell amplitude. In both the P_{11} an P_{33} channels it is clear from the results that the separable expansion gives an accurate representation of the πN amplitude calculated in Ref. 15.

The πB and πB^* propagators τ_B and τ_{B^*} arise from the pole and nonpole parts, respectively, of the πB input amplitude $\bar{T}^{(0)}$. The resultant amplitude for the partial wave γ is given by

$$\bar{T}^{(1)\gamma}_{\alpha\beta}(p,p';E)=\sum_{i,j}\phi^{\gamma}_{i}(\alpha,p)\tau^{ij}_{\gamma}(E)\phi^{\gamma}_{j}(\beta,p') . \quad (3.11)$$

The matrix τ_γ (which is actually the πB^* propagator τ_{B^*} corresponding to a B^* in partial wave γ) is given by

$$\tau^{-1}_{\gamma}(E)=\Lambda^{-1}_{\gamma}(E)-\langle\phi^{\gamma}|g(E)|\phi^{\gamma}\rangle \quad (3.12)$$

with the propagator g being the same as that used in Ref. 15. The matrix τ describes the propagation of the πB resonance B^* in the presence of a spectating pion. The matrix $\langle\phi^{\gamma}|g(E)|\phi^{\gamma}\rangle$ is a square matrix of rank equal to the rank of the expansion with elements given by

$$\langle\phi_{\gamma}|g(E)|\phi_{\gamma}\rangle_{ij}=\sum_{\alpha}\int_0^{\infty}dp\,p^2\phi^{\gamma}_{i}(\alpha,p)g_{\alpha}(p;E)\phi^{\gamma}_{j}(\alpha,p) . \quad (3.13)$$

Using Eq. (3.11) in Eq. (2.2) and expanding out the matrix nature of the equation gives

$$\bar{f}^{(1)}_{\pi\alpha\beta}(p;E)=\bar{f}^{(2)}_{\pi\alpha\beta}(p)+\sum_{i,j}\phi^{\beta}_{i}(\alpha;p)\tau^{ij}_{\beta}(E)\times\sum_{\gamma}\int_0^{\infty}dp'p'^2\phi^{\beta}_{j}(\gamma;p')\times g_{\gamma}(p';E)\bar{f}^{(2)}_{\pi\gamma\beta}(p') . \quad (3.14)$$

In this equation, the label β labels a baryon when appearing as a subscript to $\bar{f}$ and the corresponding B^* channel when labeling ϕ and τ.

For the πB channels we need to define the diagonal matrix τ_B. This arises from the pole part of the amplitude obtained by iterating the potential of Eq. (3.9).

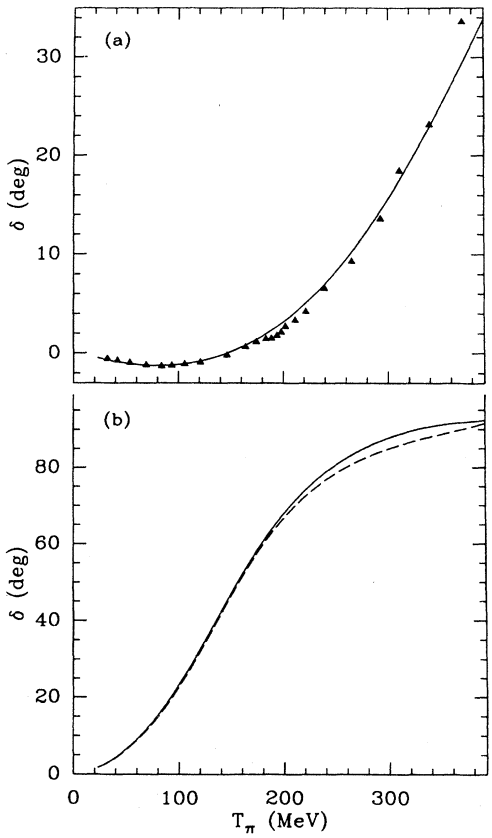

FIG. 6. The two-body input in the P_{11} channel. The total phase shifts are shown in (a) while the nonpole are in (b). The data in (a) are from Ref. 27 while the dashed curve in (b) comes from the calculation of Ref. 15.

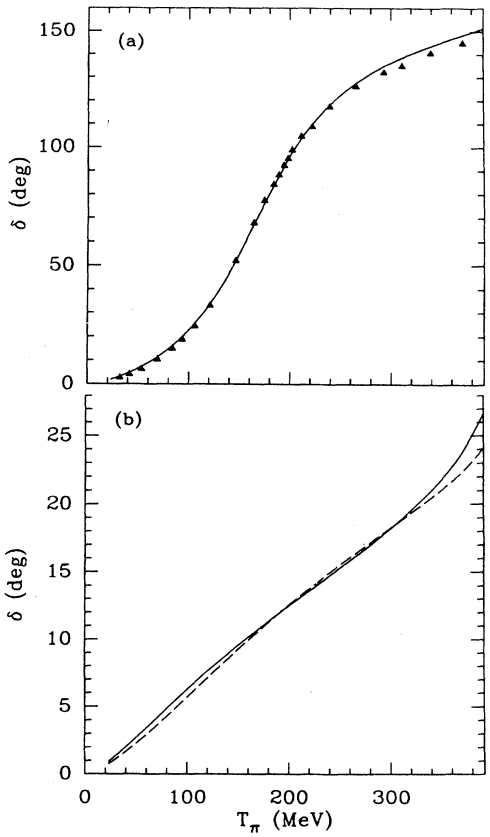

FIG. 7. Same as Fig. 6 but for the P_{33} input.

From Eq. (A2) we know that τ_B is just the dressed baryon propagator in the presence of another pion. Hence we have the elements of τ_B given by

$$\tau_\alpha(E)=[E-\overline{m}_{0\alpha}-\overline{\Sigma}^{(1)}_\alpha(E)]^{-1}$$
$$=\Big[E-\overline{m}_{0\alpha}-\sum_\beta\int_0^\infty dp\,p^2\overline{f}^{(2)}_{\alpha\beta\pi}(p)g_\beta(p;E)\times\overline{f}^{(1)}_{\pi\beta\alpha}(p;E)\Big]^{-1}, \quad (3.15)$$

with the function $\overline{f}^{(1)}$ given by Eq. (3.14). From Ref. 15 we know that Eq. (3.15) for $\alpha=N$ can be written in the form

$$\tau_N(E)=\frac{\overline{Z}_{2N}}{(E-m_N)[1-(E-m_N)\overline{Z}_{2N}\overline{\Sigma}_{2N}(E)]}, \quad (3.16)$$

where $\overline{\Sigma}_{2N}$ arises from an expansion of the form given in Ref. 15. Hence, $\tau_N(E-e_N(p))$ has residue $\overline{Z}_{2N}$ at the πN on-shell pole [the energy function $e_N(p)$ is defined later in Eq. (3.21)]. Since $\tau_N(E-e_N(p))$ plays the role of a πN propagator in the integral equation of Eq. (A6), the factor of $\overline{Z}_{2N}$ must be taken into account when extracting the phase shift and inelasticity from the amplitude X_{NN}.

The πB-$\pi\pi B$ equations we have presented include coupling to channels in which the two pions interact while the nucleon or delta is a spectator (see Fig. 5). This is included via the $\pi\pi$ amplitude that first appears in Eq. (2.11). In principle, this amplitude can be obtained by iterating the $\pi\pi$ interaction present in the cloudy bag model Lagrangian in a Lippmann-Schwinger equation. For this calculation, however, we choose to use instead a phenomenological fit to the $\pi\pi$ scattering data. This ensures that we correctly include the thresholds generated by the $\pi\pi$ resonances in the $(t,j)=(0,0)$ and $(1,1)$ channels. The effects of using the cloudy bag model description of the $\pi\pi$ interaction can be studied at a later date. Johnstone and Lee[28] use a similar approach in their study of the importance of $\pi\pi$ correlations in πN scattering, and we use their $\pi\pi$ parametrization here. The potential $\overline{T}^{(2)}(3)$ that we use in Eq. (2.12) is

$$\overline{T}^{(2)}(3)(p,p';E)=\frac{\overline{f}_\rho(p)\overline{f}_\rho(p')}{E-m_{0\rho}}, \quad (3.17)$$

with the form factor [which also appears in the crossed diagram; see Eqs. (A13) and (2.9)] given by

$$\overline{f}_\rho(p)=\frac{cp^j}{(1+p^2/\beta^2)^{j+1}}. \quad (3.18)$$

With this separable potential the one-particle irreducible $\pi\pi$ amplitude is easily found to be

$$\overline{T}^{(1)}(3)(p,p';E)=\overline{f}_\rho(p)\tau_\rho(E)\overline{f}_\rho(p'), \quad (3.19)$$

with

$$\tau_\rho(E)=\left[E-m_{0\rho}-\int_0^\infty dp\,p^2\frac{\overline{f}^2_\rho(p)}{E-2\omega_p}\right]^{-1}. \quad (3.20)$$

TABLE III. The parameters for the $\pi\pi$ input (from Ref. 28).

(t,j)	c (fm$^{j+1/2}$)	β (fm^{-1})	$m_{0\rho}$ (meV)
(0,0)	0.9051	1.916	896.8
(1,1)	0.3430	2.336	811.7

The parameters for the $(t,j)=(0,0)$ and $(1,1)$ resonances are listed in Table III. The phase shifts for these parametrizations can be seen in Ref. 28.

The function τ_ρ appears in the three-body equations, Eq. (A6) in conjunction with a B propagator d [see Eq. (2.11)]. Hence the τ_ρ appearing in Eq. (A6) is actually a block diagonal matrix with one element corresponding to ρN propagation and the other to $\rho\Delta$.[20,26]

Each of the τ functions appearing in Eq. (A6) has an energy argument of the form $E-e_\lambda(p)$ where E is the three-body c.m. energy and p is the integration momentum. With the choice of relativistic kinematics that we use, the subsystem energy $e_\lambda(p)$ is defined by

$$e_B(p)=(p^2+m_\pi^2)^{1/2}+(p^2+m_B^2)^{1/2}-m_B, \quad (3.21a)$$

$$e_{B^*}(p)=(p^2+m_\pi^2)^{1/2}+(p^2+m_{B^*}^2)^{1/2}-m_{B^*}, \quad (3.21b)$$

$$e_{\rho(\alpha)}(p)=(p^2+m_\alpha^2)^{1/2}+[p^2+(2m_\pi)^2]^{1/2}-2m_\pi. \quad (3.21c)$$

For the ρ channels, the α labels the spectating baryon. If the B^* has the same quantum numbers as a baryon channel B, then we take m_{B^*} to be the mass of that baryon. Otherwise we take $m_{B^*}=m_N+m_\pi$. This choice ensures that the thresholds appear at the correct energies.

The numerical solution of three-body equations has by now become routine. The main difficulty that arises is to ensure that all singularities of the kernel are avoided. We use the technique of contour deformation to avoid these singularities, with the contour shown in Fig. 8. The contour must eventually return to the real axis. This restriction is caused by the Bessel functions that appear in the contact term which would oscillate wildly if the imaginary part of the integration momentum extended to infinity.

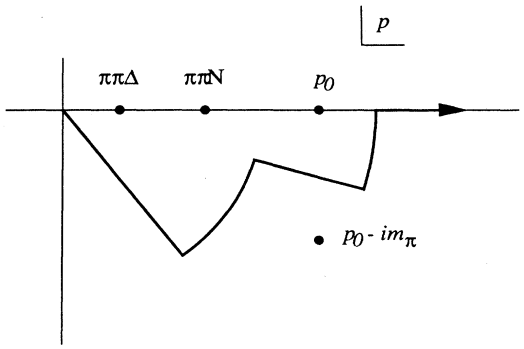

FIG. 8. The contour of integration.

On the real axis we must avoid the on-shell momentum p_0 and logarithmic singularities arising from the $\pi\pi N$ and $\pi\pi\Delta$ thresholds, which are always at smaller momenta than p_0. Away from the real axis the most restrictive singularity is a square-root branch point from the half-on-shell π-exchange amplitude at $p_0 - im_\pi$. As illustrated in Fig. 8, the contour we choose avoids all of these. We find it necessary to use a total of 36 Gaussian quadratures distributed along this contour.

IV. RENORMALIZATION

In this section we discuss the renormalization procedure. Although this has been discussed thoroughly in Ref. 15 for the two-body equations, there are some subtleties specific to the three-body equations. Specifically, care must be taken since we have two different levels of baryon dressing. A single baryon—the baryon appearing in the pole diagram—is dressed by solving the three-body equations. It will receive dressing from diagrams like that shown in Fig. 9 (although we expect such contributions to be small). On the other hand, the baryon in a πB intermediate state will not receive dressing from such contributions. Its dressing is determined by the separable approximation to the low energy solution discussed in the preceding section.

We will discuss here only the case when the Roper is excluded from the single baryon space. Including the Roper simply means we must follow the procedure outlined in Ref. 15 in order to diagonalize the dressed single baryon propagator.

The renormalization procedure is driven by requiring that the scattering amplitude have a pole at the physical nucleon mass and that the residue at that pole reproduce the physical πNN coupling constant. From Eqs. (2.1), (2.3), and (A5), the requirement that there be a pole in the P_{11} partial wave of X_{BB} at the physical nucleon mass simply means

$$d^{-1}(m_N) = d_0^{-1}(m_N) - \Sigma^{(1)}(m_N) = 0 , \tag{4.1}$$

or

$$m_{0N} = m_N - \Sigma^{(1)}_{NN} . \tag{4.2}$$

The residue of the dressed baryon propagator at this pole is Z_{2N} where

$$Z_{2N} = \left[1 - \frac{\partial}{\partial E} \Sigma^{(1)}_{NN}(m_N) \right]^{-1} . \tag{4.3}$$

To extract the renormalized coupling constant, we must put the external legs of the $\pi N \to \pi N$ amplitude on shell and take the residue at the nucleon pole. However, when we put the external legs on shell we gain a factor of $\bar{Z}_{2N}$ coming from the πB propagator. That is, we have different baryon renormalization constants coming from the single baryon propagator and the πB propagator since the degree of renormalization is different in each case. Hence the relationship between the renormalized coupling constant $f^R_{\pi NN}$ and the bare coupling constant f_0 that enters into the pole diagram is[15]

$$f^R_{\pi NN} = f_0 \frac{f^{(1)}_{\pi NN}(p_0; m_N)}{f^{(2)}_{\pi NN}(p_0)} Z^{1/2}_{2N} \bar{Z}^{1/2}_{2N} u(p_0 R) . \tag{4.4}$$

Here p_0 is the (imaginary) on-shell momentum at the nucleon pole, R is the bag radius and $u(p_0 R)$ is the bag vertex function. Since $\Sigma^{(1)}$ is proportional to f_0^2, this can be solved to find the value of f_0 that gives $f^{R2}_{\pi NN} = 0.08$. Then Eq. (4.2) can be used to determine the bare nucleon mass.

When a Roper pole diagram is included we must diagonalize the baryon propagator using the procedure outlined in Ref. 15. In this case, we add the constraint that the P_{11} phase shifts go through 90° at the Roper resonance energy in order to fix the bare Roper mass.

V. DISCUSSION AND RESULTS

We are now in a position to begin calculations of the πN amplitudes at energies above the pion production threshold. At this stage, our interest is primarily in the P_{11} channel in the region of the Roper resonance. From the *Review of Particle Properties*[7] the important decay modes of the Roper are πN (50–70 %), $\pi\Delta$ (10–20 %), ρN (10–15 %), and $(\pi\pi)_S N$ (5–20 %). All of these thresholds are included in our calculation. However, if we include a bare Roper pole diagram then we are missing some of the contribution for decay to ρN and $(\pi\pi)_S N$ since we do not have a direct vertex for $R \to \rho N$ or $R \to \pi\pi N$. In summary, the set of coupled equations we solve are Eqs. (A6). The driving terms are given by Eqs. (A12) and (A13) with the two-body input described in Sec. III.

When including the pole, crossed, and contact dia-

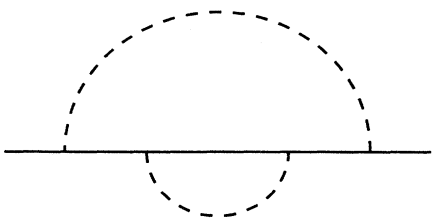

FIG. 9. A diagram that contributes to baryon dressing in single baryon states but not in πB states.

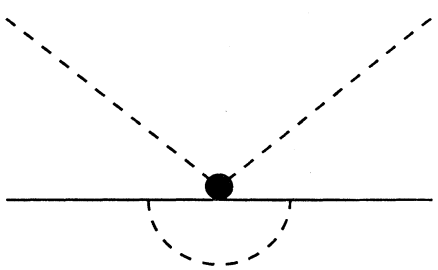

FIG. 10. A diagram that dresses the contact diagram.

grams through Eq. (A12) we must give some consideration to the value we choose for their strengths. We expect that, at low energies, this calculation will be an extension of the two-body calculation reported in Ref. 15. However, in that case the residue of the πB propagator at the on-shell pole was unity while now it is $\bar{Z}_2$, a consequence of dressing the baryon in the πB intermediate state. This means we must examine the strengths of the diagrams to ensure we are being consistent. For the case of the crossed diagram, the extra factor is just what is needed to ensure that the vertices reproduce the experimental coupling constant. Since in Ref. 15 we used this criterion when setting the strengths of these vertices, we have ensured consistency in the crossed diagram. Similarly, the strength of the pole diagram is fixed in both cases by insisting that the residue at the nucleon pole

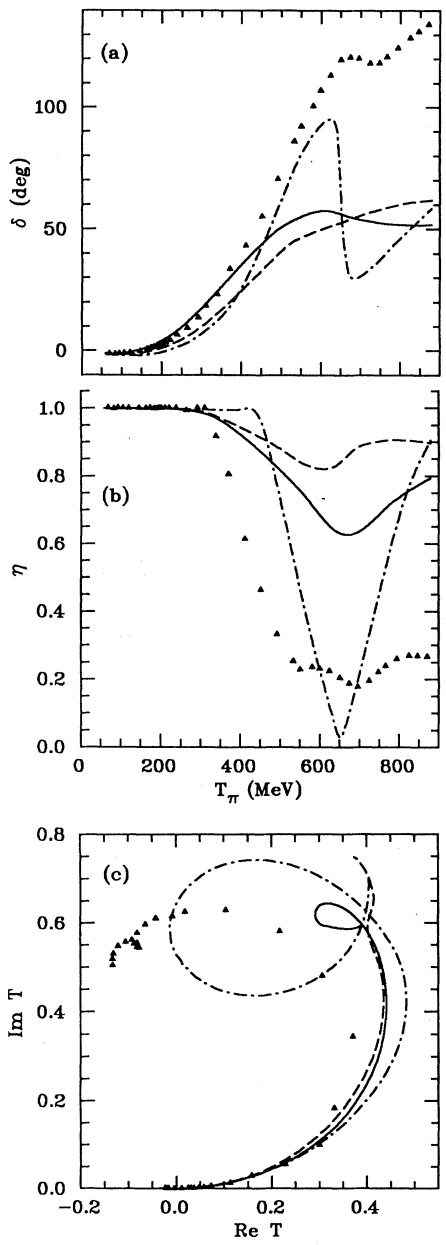

FIG. 11. Results for the P_{11} phase shifts (a), inelasticity (b), and Argand diagram (c) with no bare Roper diagram. All curves have $f_\pi = 80$ MeV. The solid curve has $R = 1$ fm, the dashed has $R = 0.9$ fm, and the dash-dotted curve has $R = 0.8$ fm. The data are from Ref. 27.

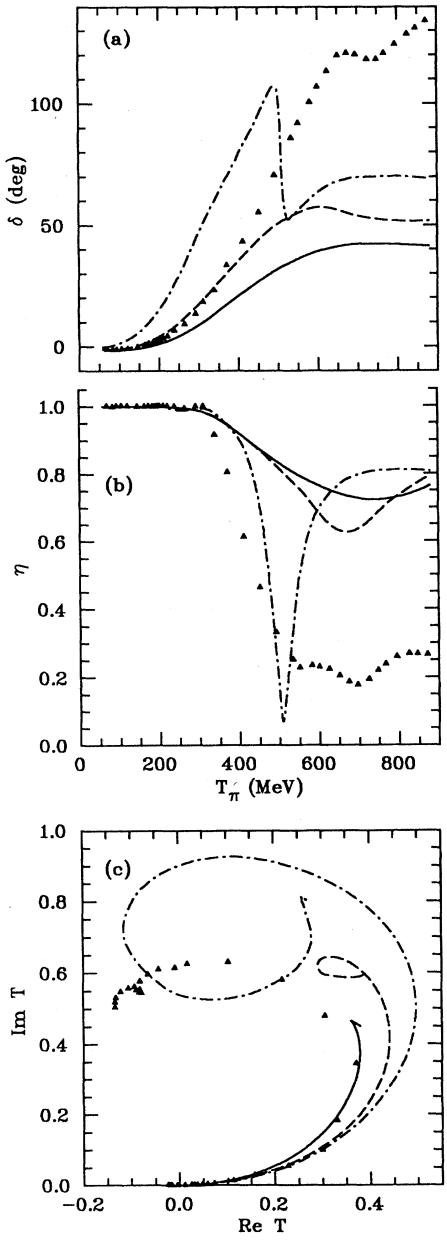

FIG. 12. Results for the P_{11} phase shifts (a), inelasticity (b), and Argand diagram (c) with no bare Roper diagram. All curves have $R = 1$ fm. The solid curve has $f_\pi = 90$ MeV, the dashed has $f_\pi = 80$ MeV, and the dash-dotted curve has $f_\pi = 70$ MeV. The data are from Ref. 27.

TABLE IV. Three-body channels included in the P_{11} calculation.

Channel No.	Two-body interaction	l	j	t	S	L	Spectator
1	N	1	$\frac{1}{2}$	$\frac{1}{2}$	$\frac{1}{2}$	1	π
2,3	P_{11}	1	$\frac{1}{2}$	$\frac{1}{2}$	$\frac{1}{2}$	1	π
4	Δ	1	$\frac{3}{2}$	$\frac{3}{2}$	$\frac{3}{2}$	1	π
5	P_{33}	1	$\frac{3}{2}$	$\frac{3}{2}$	$\frac{3}{2}$	1	π
6	S^*	0	0	0	$\frac{1}{2}$	0	N
7	ρ	1	1	1	$\frac{1}{2}$	1	N
8	ρ	1	1	1	$\frac{3}{2}$	1	N

reproduce the physical coupling constant. However, the effective strength of the contact diagram in this case is a factor of $\bar{Z}_2$ different than in Ref. 15. Hence we would need to increase the bare contact diagram by $\bar{Z}_{2N}^{-1}$ in order to maintain consistency with the previous calculation. This translates to using $f_\pi = 80$ MeV in the contact diagram instead of $f_\pi = 90$ MeV. However, we observe that the single scattering term $Z_{BB^*}\tau_{B^*}Z_{B^*B}$ includes a contribution from the diagram in Fig. 10 which dresses the bare contact diagram. Hence we consider the strength of the bare contact diagram, $1/f_\pi^2$, as a parameter. However, we note that the best results were achieved using $f_\pi \sim 80$ which suggests that the renormalization due to Fig. 10 is small. We note that f_π and the bag radius R are the only two parameters in the calculation.

In order to see if the Roper resonance can be described simply by the coupling to the inelastic channels, we begin by examining the results in the P_{11} channel in the absence of any bare Roper pole diagram. The eight coupled channels included in the calculation are listed in Table IV. In Fig. 11 we show the results for a range of the bag radius parameter R with the strength of the contact diagram fixed by $f_\pi = 80$ MeV. The solid curve has $R = 1$ fm, the dashed curve has $R = 0.9$ fm, and the dash-dotted curve has $R = 0.8$ fm. The effect of varying f_π can be seen in Fig. 12. Here R is set to 1 fm while the solid curve has $f_\pi = 90$ MeV, the dashed curve has $f_\pi = 80$ MeV, and the dash-dotted curve has $f_\pi = 70$ MeV. The strange structure of the phase shifts when the radius is decreased and when the strength of the contact diagram is increased becomes less puzzling if one looks at the Argand diagrams. Here we see that there is a gradual widening of the loop until it almost encircles the point $(0,\frac{1}{2})$. Hence we see that strong resonance behavior is exhibited for a small bag radius or for a strong contact diagram. However, this behavior is not in good quantitative agreement with the data.

TABLE V. Renormalization results with no bare Roper diagram.

R (fm)	f_π (MeV)	f_0^2	m_{0N} (MeV)	Z_{2N}
1.0	90	0.050 75	1112.3	0.7067
1.0	80	0.042 07	1109.0	0.6799
1.0	70	0.028 97	1101.3	0.6242
0.9	80	0.034 13	1188.5	0.5592
0.8	80	0.026 29	1433.7	0.2944

The bare πNN coupling constant, bare nucleon mass, and nucleon wave function normalization determined from the renormalization procedure are tabulated in Table V for each case discussed above.

Although the calculation does not produce good quantitative agreement with the experimental data, the qualitative features are rather interesting. Firstly we note from Fig. 12 that the contact diagram is capable of producing a very strong and narrow resonance. Since this resonance occurs just above the $\pi\Delta$ threshold we suspect that the contact diagram may be producing a narrow $\pi\Delta$ resonance. Also we notice that we have the correct mechanisms necessary to explain the dip in the inelasticity that corresponds to the opening of the $\pi\pi N$ threshold at $T_{\text{lab}} = 170$ MeV. We observe that this structure is sensitive to the bag radius and prefers a larger radius.

We now consider the effects of including a bare Roper pole diagram. We can include the Roper using either the [56] representation in which the spatial part of the wave function is totally symmetric, or using the [70] representation corresponding to a spatial wave function of mixed symmetry. We now add to the renormalization procedure the constraint that the P_{11} phase shifts go through

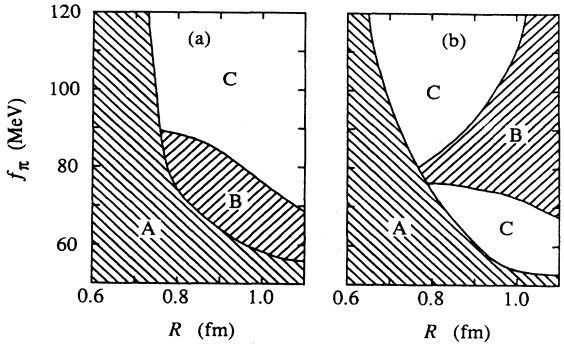

FIG. 13. The region of parameter space in which all renormalization constraints *cannot* be satisfied (shaded regions) when the Roper is included in the (a) [56] and (b) [70] representations.

90° at the Roper resonance energy. Hence we are now placing three constraints on the amplitude in the P_{11} channel. These are (a) there must be a pole at the nucleon mass, (b) the residue at that pole must give the physical πNN coupling constant, and (c) there must be a resonance at the Roper resonance (although the width is not constrained). Perhaps not surprisingly, we find that there are some values of the parameters R and f_π where it is impossible to satisfy all of these constraints. In Fig. 13 we show the region of parameter space in which all these constraints can be satisfied (the unshaded regions C) for the case of the [56] [Fig. 13(a)] and [70] [Fig. 13(b)] representations. For parameters in the shaded region A, it is impossible to find a value of the bare coupling constant that will reproduce the physical value of $f^2_{\pi NN}=0.08$ for any value of the bare Roper mass. In region B, this can be achieved but it is not possible to find a value for the bare Roper mass that will produce a resonance at the right energy. The constraint that there must be a resonance at the Roper position effectively screens out values of the parameters that produce phase shifts that bear little resemblance to experiment. As we can see, using the [70] representation constrains the parameters much more than does the [56] representation.

In Figs. 14 and 15 we show the P_{11} results when the [56] representation of the Roper is used, for a fixed value of f_π and a range of bag radii (Fig. 14) and for a fixed bag radius and two values of f_π (Fig. 15). The values of the bare masses and coupling constants are given in Table VI. Figure 14 has f_π fixed at 90 MeV with $R=1.0$ fm (solid curve), $R=0.9$ fm (dashed curve), and $R=0.8$ fm (dash-dotted curve). These curves show that the width of the Roper is somewhat sensitive to the bag radius, preferring a larger radius. We also note that the phase shifts continue to rise after passing through 90° and actually continue through 180°. In Fig. 15 we have the results for a bag radius of 1 fm with $f_\pi=90$ MeV (solid curve) and $f_\pi=80$ MeV (dashed curve). Up to a lab energy of around 600 MeV, the calculation with $f_\pi=80$ MeV shows reasonable agreement with the Karlsruhe-Helsinki phase shift analysis,[27] but at higher energy there is a significant disagreement, with the phase shifts again going through 180°.

We now explore the consequences of using the [70] representation of the Roper. As noted, we are now more restricted in the ranges of the two parameters [see Fig. 13(b)]. We show in Fig. 16 the results for $R=0.8$ fm with $f_\pi=90$ MeV (solid curve) and $f_\pi=85$ MeV (dashed curve). We had expected that the [70] representation would give a larger width to the resonance[29] which is

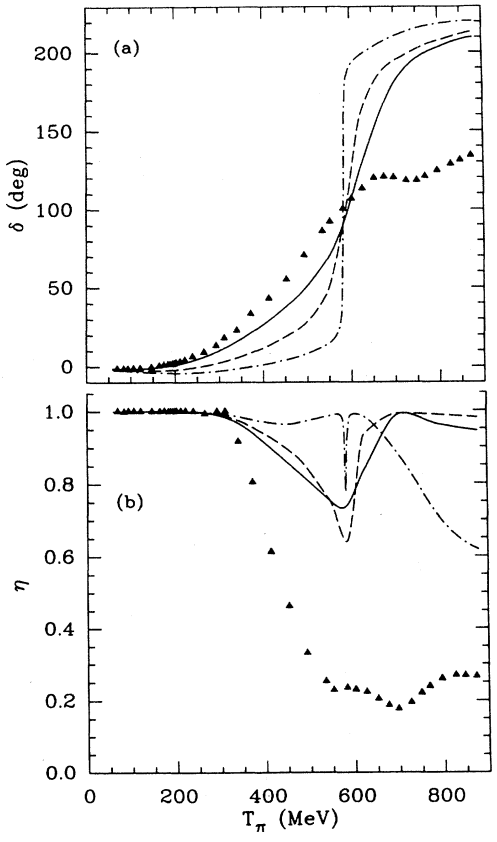

FIG. 14. P_{11} results when a bare Roper is included using the [56] representation and $f_\pi=90$ MeV. The solid curve has $R=1$ fm, the dashed has $R=0.9$ fm, and the dash-dotted curve has $R=0.8$ fm. The data are from Ref. 27.

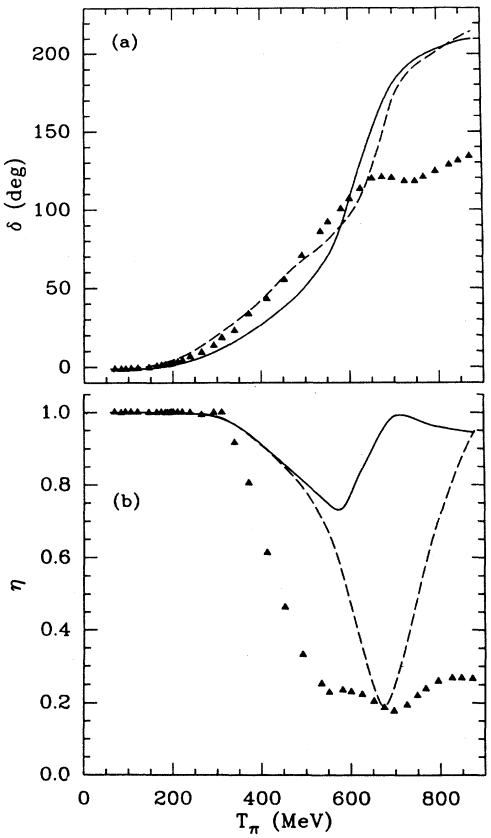

FIG. 15. P_{11} results when a bare Roper is included using the [56] representation and $R=1$ fm. The solid curve has $f_\pi=90$ MeV and the dashed curve has $f_\pi=80$ MeV. The data are from Ref. 27.

indeed borne out by these calculations (compare the solid curve of Fig. 16 with the dash-dotted curve of Fig. 14). However, in the case of the [70] calculation, we are unable to find a value of the bare Roper mass that gives a resonance at the correct energy for a large bag radius. At the smaller bag radii, the inelasticity in the vicinity of the Roper is poorly reproduced.

To illustrate the effect of dropping our insistence that there be a resonance at the Roper energy, we show in Fig. 17 a calculation using the [70] representation with $R=1$ fm and $f_\pi=80$ MeV. Here we use a "reasonable" value of 1600 MeV for the bare Roper mass. The other bare values are given in Table VI. This explains why it was not possible to find a value of the bare Roper mass that would force the phase shifts through 90° at the Roper resonance. The reason is that, for these values of R and f_π the Argand diagram loops too strongly and never crosses the imaginary axis.

Part of the motivation for this project was to see if the Roper resonance could be reproduced without actually having a bare Roper three-quark state. That is, we wanted to see if the nearby $\pi\pi N$, $\pi\Delta$, and ρN thresholds and the strength of the πN interaction could combine to produce the observed resonant behavior. For this purpose the model we have solved contains all the important ingredients. Specifically, it has all of the above-mentioned thresholds (included via the exchange diagrams of Figs. 4 and 5) and the low energy behavior has been shown to be good.[15] As we have seen, resonant behavior is possible although not in detailed agreement with the data. If this then means that a bare Roper three-quark state is needed then our calculation is missing one ingredient. That is

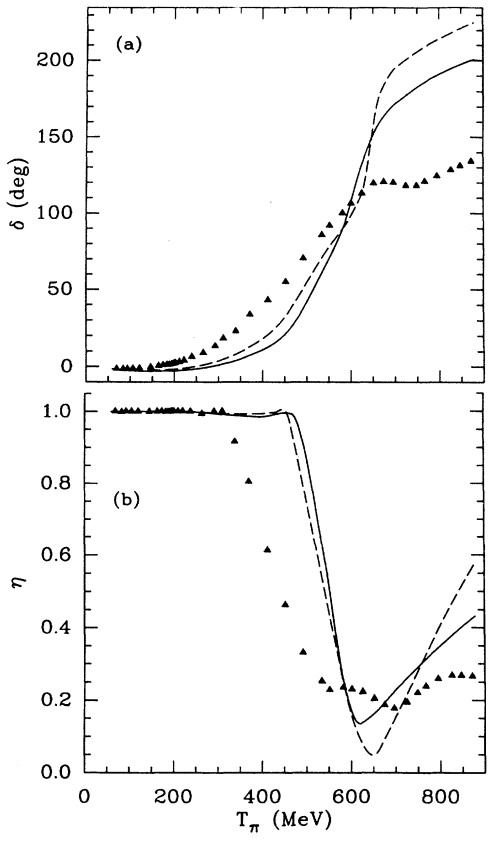

FIG. 16. P_{11} results when a bare Roper is included using the [70] representation and $R=0.8$ fm. The solid curve has $f_\pi=90$ MeV, and the dashed curve has $f_\pi=85$ MeV. The data are from Ref. 27.

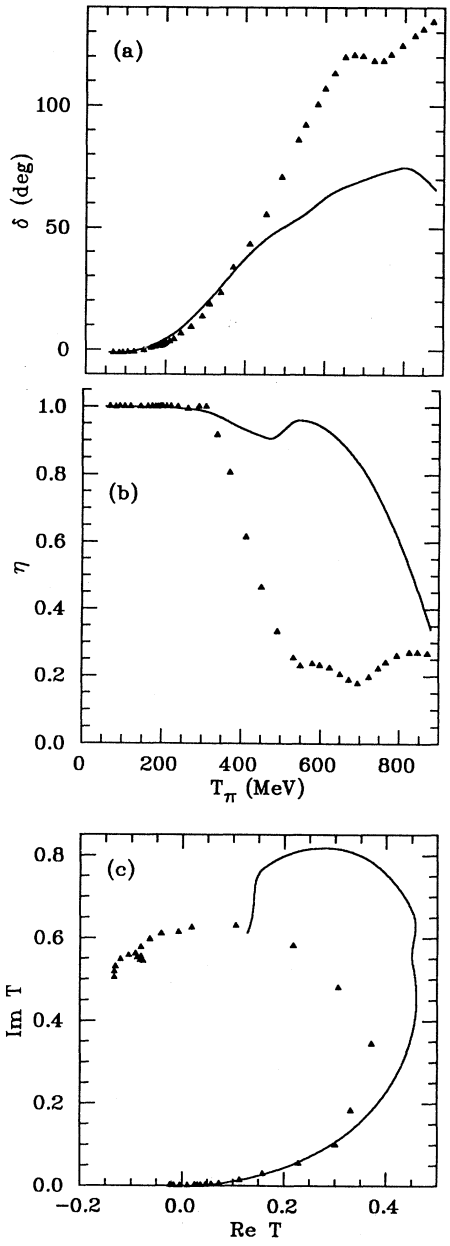

FIG. 17. Case where the P_{11} phase shifts do not go through 90° despite having a bare [70] Roper pole term. $f_\pi=80$ meV and $R=1$ fm.

TABLE VI. Renormalization results with the bare Roper diagram included.

Roper type	R (fm)	f_π (MeV)	f_0^2	m_{0N} (MeV)	Z_{2N}	m_{0R} (MeV)
[56]	1.0	90	0.049 22	1115.7	0.6965	1580.1
[56]	1.0	80	0.040 71	1111.3	0.6705	1639.8
[56]	0.9	90	0.043 75	1202.6	0.5955	1576.7
[56]	0.8	90	0.040 16	1437.5	0.4117	1527.0
[70]	0.8	90	0.040 06	1369.4	0.4493	1704.3
[70]	0.8	85	0.033 97	1390.8	0.3898	1811.9
[56][a]	1.0	80	0.041 71	1115.8	0.6664	1589.4
[70][b]	1.0	80	0.042 19	1109.6	0.6793	1600.0

[a]No coupling to $\pi\pi$ channels.
[b]Not constrained to give resonance.

the ability for the Roper bag to decay directly to ρN and $(\pi\pi)_S N$. This would be included if we were able to include the $B \to \pi\pi B$ vertex and deserves further investigation.

It is interesting to consider the relative importance of the $\pi\pi$ interaction to the calculation. In Fig. 18 we show the effects of neglecting the $\pi\pi$ channels for $R=1$ fm and $f_\pi=80$ MeV and using the [56] representation. That is, we only include channels 1–5 from Table IV. The solid curve includes the $\pi\pi$ channels while in the dashed curve they are omitted. Clearly the effect on the phase shifts is minimal while the inelasticity is affected dramatically.

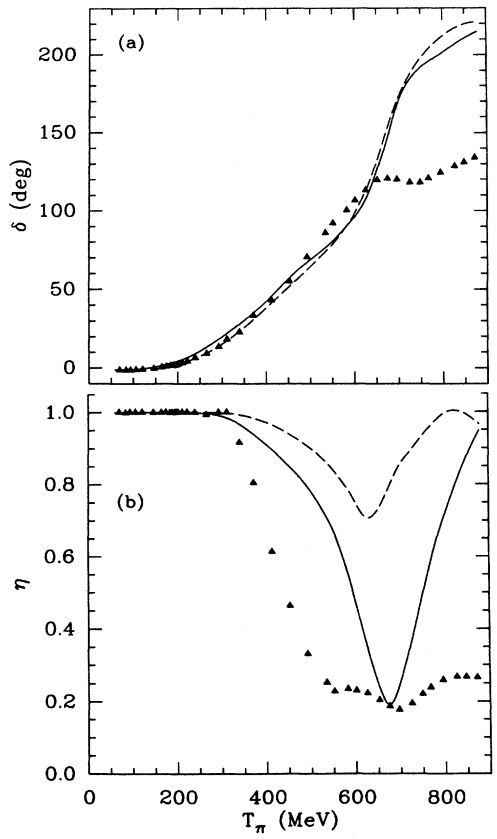

FIG. 18. P_{11} results with (solid curve) and without (dashed curve) the $\pi\pi$ channels. $f_\pi=80$ MeV and $R=1$ fm and a bare [56] Roper pole.

VI. CONCLUSION

In this paper we have presented the details of a scheme for calculating the pion-nucleon scattering amplitudes from the cloudy bag model Lagrangian (or any similar chiral Lagrangian). This scheme is in the form of a set of coupled integral equations (derived in Ref. 17) whose input is specified by the given Lagrangian. The resultant amplitude in the P_{11} channel has the correct position for the nucleon pole, and the value of the residue at this pole, i.e., the πNN coupling constant. This same amplitude also satisfies two- and three-body unitarity. This implies that we have included the thresholds for the reactions $\pi N \to \pi\pi N$, ρN, and $\pi\Delta$. To the best of our knowledge, this is the first calculation that achieves these three goals. In the development of these equations, the basic interactions are taken from some Lagrangian. In our case we have used the version of the cloudy bag model Lagrangian in which the pions interact throughout the bag volume.[8–11] However, to keep the equations manageable, we have made a number of approximations. (i) We have neglected contributions from the Lagrangian that change the number of pions by two or more. Such contributions could be included in perturbation theory. Neglecting these terms means that the interactions we use are the $B \to \pi B$ vertex and the $\pi B \to \pi B$ contact term. This also implies that on inclusion of the Roper as a radially excited three-quark state, we do not allow this Roper bag state to decay directly into a ρN and $(\pi\pi)_S N$. (ii) We have assumed that the original chiral Lagrangian at the quark level can be truncated to include only the lowest order terms in the pion field. This approximation, which was implemented to get the cloudy bag model, is valid for large bag radii ($R \approx 1$ fm), where the multipion contribution to the physical nucleon is negligible.[30] (iii) Since the bare masses and coupling constant are set by the renormalization procedure, the only two parameters in the calculation are the bag radius and the strength of the contact diagram (proportional to f_π^{-2}). We have used the

bag radius as a parameter in the present calculation. As for the strength of the contact term, it should, after renormalization, be the pion decay constant for chiral symmetry to be satisfied. However, the solution of the coupled equations contributes to the renormalization, and at this stage it is difficult to determine the contribution from this renormalization. We therefore were forced to treat the strength of the contact term as a parameter.

In the present investigation we have considered the possibility of including in our calculation a radially excited three-quark state (the bare Roper bag), or not including any such state. In this way we hoped to determine if the $N^*(1470)$ has a three-quark component. In general, we find we have better agreement with the experimental phase shifts in the absence of a bare Roper bag. This is the case when we include either the symmetric [56] representation, or the mixed symmetry [70] representation. In particular, we find that the inclusion of the bare Roper bag causes the P_{11} phase shifts to go through 180°. This is inconsistent with the observed data, suggesting that the $N^*(1470)$ is predominantly due to dynamic effects, and has little contribution from a bare Roper bag. Our conclusion is supported by the fact that all attempts at including the bare Roper bag into the calculation of the P_{11} phase shifts lead to rapid changes in the phases in the vicinity of the resonance which indicates that the width of a Roper bag would be too small as compared to the observed width. The suggestion that we should include both the [56] and [70] representation does not overcome this problem. In fact, if anything, it would make things worse, since the coupling between the two resonances has the effect of reducing the width of the [56] representation even further, thus making the discrepancy between theory and experiment larger. One possible solution to the question of the role of a radially excited three-quark bag is to associate this state with the $N^*(1720)$.

Finally, if we take into consideration the fact that we have truncated our Lagrangian to the extent of including only the lowest order terms in the pion field, not included the $q \rightarrow q\pi\pi$ coupling in the Lagrangian, and the fact that the cloudy bag model is the simplest of the chiral bag models, the agreement between theory and experiment is remarkably good. Also we note that we reproduce at one end of the energy scale, both the nucleon pole position and its residue, while at the other end of the scale we reproduce the thresholds for pion, Δ, and ρ production, without having a parameter search.

APPENDIX: SEPARABLE INTERACTIONS AND SYMMETRIZATION

For practical applications, we must write the three-body equations of Sec. II [see Eqs. (2.13)–(2.15)] for the case of separable two-body interactions. The technique for doing this is similar to that used for the πNN equations.[18,19] We begin by writing the $3 \rightarrow 3$ amplitudes, $M_d^{(2)}(\lambda)$ in separable form as

$$M_d^{(2)}(j) = |\pi_{\bar{j}} B_j^* \rangle \tau_{B^*} \langle \pi_{\bar{j}} B_j^* | \ , \tag{A1a}$$

$$M_d^{(2)}(3) = |\rho B \rangle \tau_\rho \langle \rho B| \ . \tag{A1b}$$

Here, $\bar{j}$ is used to denote the pion other than pion j. We denote a πB subinteraction by B^* and a $\pi\pi$ interaction by ρ. Separable subinteractions of arbitrary rank are possible by letting the form factors and τ functions above be matrices. If the B^* subinteraction is to be rank N_{B^*} and $B = N, \Delta$, then $|\pi_{\bar{j}} B_j^* \rangle$ will be a $2 \times N_{B^*}$ matrix and τ_{B^*} will be a $N_{B^*} \times N_{B^*}$ matrix. From Eq. (2.11) we see that $M_d^{(2)}(3)$ must be a 2×2 matrix due to the spectating baryon. Hence, if the rank of the $\pi\pi$ interaction is N_ρ then $|\rho B \rangle$ will be a $2 \times 2N_\rho$ matrix and τ_ρ will be a block diagonal $2N_\rho \times 2N_\rho$ matrix, the two diagonal blocks corresponding, respectively, to an N and Δ spectator.[20,26] We also introduce plane wave bases for the $\pi_i B$ system that are eigenstates of the πB propagator, i.e.,

$$g|\pi_i B \rangle = \tau_B |\pi_i B \rangle \ . \tag{A2}$$

These must satisfy the completeness relation

$$\sum_i |\pi_i B \rangle \langle \pi_i B| = 1 \ . \tag{A3}$$

Note that both τ_B and $|\pi_i B \rangle$ are 2×2 diagonal matrices. The physical wave functions are defined by symmetrizing with respect to interchange of pion labels. That is,

$$|\pi B \rangle^S = \frac{1}{\sqrt{2}} (|\pi_1 B \rangle + |\pi_2 B \rangle) \ , \tag{A4a}$$

$$|\pi B^* \rangle^S = \frac{1}{\sqrt{2}} (|\pi_1 B_2^* \rangle + \pi_2 B_1^* \rangle) \ , \tag{A4b}$$

$$|\rho B \rangle^S = |\rho B \rangle \ . \tag{A4c}$$

The physical amplitudes can then be written down by taking matrix elements of the $T^{(0)}$ amplitudes with respect to these wave functions. We define

$$X_{BB} = {}^S\langle \pi B | T_{BB}^{(0)} | \pi B \rangle^S \ , \tag{A5a}$$

$$X_{B^*B} = \sum_i {}^S\langle \pi B^* | G T_{iB}^{(0)} | \pi B \rangle^S$$
$$= \frac{1}{\sqrt{2}} (\langle \pi_1 B_2^* | G T_{2B}^{(0)} | \pi B \rangle^S + \langle \pi_2 B_1^* | G T_{1B}^{(0)} | \pi B \rangle^S) \ , \tag{A5b}$$

$$X_{\rho B} = {}^S\langle \rho B | G T_{3B}^{(0)} | \pi B \rangle^S \ . \tag{A5c}$$

Here we observe that the X amplitudes are matrices, and their dimensions are dependent on the rank of the separable input amplitudes. For example, if we take $B = N, \Delta$, then X_{BB} is always a 2×2 matrix, while X_{B^*B} is an $N_{B^*} \times 2$ matrix, where N_{B^*} is the rank of the B^* subamplitude. If we use these expressions in Eqs. (2.13) and (2.14) then after some algebra we have

$$X_{BB} = \nu_{BB} + \nu_{BB} \tau_B X_{BB} + Z_{BB^*} \tau_{B^*} X_{B^*B} + Z_{B\rho} \tau_\rho X_{\rho B} \ , \tag{A6a}$$

$$X_{B^*B} = Z_{B^*B} + Z_{B^*B} \tau_B X_{BB} + Z_{B^*B^*} \tau_{B^*} X_{B^*B} + Z_{B^*\rho} \tau_\rho X_{\rho B} \ , \tag{A6b}$$

$$X_{\rho B} = Z_{\rho B} + Z_{\rho B} \tau_B X_{BB} + Z_{\rho B^*} \tau_{B^*} X_{B^*B} \ . \tag{A6c}$$

In the above we have

$$\nu_{BB}={}^S\langle \pi B|V_{BB}|\pi B\rangle^S \ . \tag{A7}$$

Expressions for the Z functions are given at the end of this appendix. Some care is needed in evaluating the right-hand side of Eq. (A7). In deriving our equations, while we have been careful to explicitly show which pion is being absorbed in the disconnected $\pi\pi B\to\pi B$ amplitudes, F_d, we have made no such distinction for the $\pi B\to B$ amplitudes, f. This is fine at the two-body level when there is no necessity for such a distinction but in the three-body equations we must be more careful. This deficiency can be easily remedied by defining the f's that appear as the pole diagram's vertices to be the symmetric combination

$$f^{(2)}=\frac{1}{\sqrt{2}}[f^{(2)}(1)+f^{(2)}(2)] \ , \tag{A8}$$

where we have now explicitly indicated the pion taking part in the interaction in parentheses. Hence we find that

$$\begin{aligned}{}^S\langle \pi B|f^{(2)}&=\tfrac{1}{2}[\langle \pi_1 B|f^{(2)}(1)+\langle \pi_2 B|f^{(2)}(2)] \\ &=\langle \pi_1 B|f^{(2)}(1) \ .\end{aligned} \tag{A9}$$

The last line follows from the indistinguishability of the pions.

We also must take care when taking symmetric matrix elements of the three-particle irreducible amplitude $T^{(3)}_{BB}$. When this amplitude was introduced into the equations, we had only one pion in the initial and final state and it was not necessary to associate a label with the pion. However, now that we find it necessary to introduce particle labels in the evaluation of matrix elements, we need to guarantee that $T^{(3)}_{BB}$ is a symmetric operator in our basis, i.e.,

$$T^{(3)}_{BB}=\tfrac{1}{2}\sum_{i,j}T^{(3)}_{BB}(ij) \ , \tag{A10}$$

where $T^{(3)}_{BB}(ij)$ is the amplitude for absorbing pion i and emitting pion j. Hence we have

$${}^S\langle \pi B|T^{(3)}_{BB}|\pi B\rangle^S=\langle \pi_1 B|T^{(3)}_{BB}(11)|\pi_1 B\rangle \ . \tag{A11}$$

Putting this all together we can write

$$\begin{aligned}\nu_{BB}&=\langle \pi_1 B|f^{(2)}(1)d_0 f^{(2)}(1)|\pi_1 B\rangle \\ &\quad+\langle \pi_1 B|T^{(3)}_{BB}(11)|\pi_1 B\rangle+Z_{BB} \ .\end{aligned} \tag{A12}$$

In this equation, Z_{BB} is given by

$$\begin{aligned}Z_{BB}&={}^S\langle \pi B|\sum_{i,j}\bar{\delta}_{ij}F^{(2)}_d(i)GF^{(2)\dagger}_d(j)|\pi B\rangle^S \\ &=\langle \pi_1 B|F^{(2)}_d(2)GF^{(2)\dagger}_d(1)|\pi_2 B\rangle \ .\end{aligned} \tag{A13a}$$

Also we have

$$Z_{B^*B}=\langle \pi_1 B^*_2|GF^{(2)\dagger}_d(1)|\pi_2 B\rangle \ , \tag{A13b}$$

$$Z_{BB^*}=\langle \pi_1 B|F^{(2)}_d(2)G|\pi_2 B^*_1\rangle \ , \tag{A13c}$$

$$Z_{B^*B^*}=\langle \pi_1 B^*_2|G|\pi_2 B^*_1\rangle \ , \tag{A13d}$$

$$Z_{B\rho}=\sqrt{2}\langle \pi_1 B|F^{(2)}_d(2)G|\rho B\rangle \ , \tag{A13e}$$

$$Z_{B^*\rho}=\sqrt{2}\langle \pi_1 B^*_2|G|\rho B\rangle \ , \tag{A13f}$$

$$Z_{\rho B}=\sqrt{2}\langle \rho B|GF^{(2)\dagger}_d(1)|\pi_2 B\rangle \ , \tag{A13g}$$

$$Z_{\rho B^*}=\sqrt{2}\langle \rho B|G|\pi_2 B^*_1\rangle \ . \tag{A13h}$$

In Eqs. (A6), (A12), and (A13) we now have a set of correctly symmetrized equations for separable input interactions.

---

*Present address: TRIUMF, 4004 Wesbrook Mall, Vancouver, B.C., Canada V6T 2A3.

[1]N. Isgur and G. Karl, Phys. Lett. **72B**, 109 (1977); **74B**, 353 (1978); Phys. Rev. D **18**, 4187 (1978).
[2]S. Capstick and N. Isgur, Phys. Rev. D **34**, 2809 (1986).
[3]R. Koniuk and I. Isgur, Phys. Rev. D **21**, 1868 (1980).
[4]G. E. Brown, J. W. Durso, and M. B. Johnson, Nucl. Phys. **A397**, 447 (1983).
[5]R. Aaron, R. D. Amado, and J. E. Young, Phys. Rev. **174**, 2022 (1968); R. Aaron and R. D. Amado, Phys. Rev. Lett. **27**, 1316 (1971).
[6]B. Blankleider and G. E. Walker, Phys. Lett. **152B**, 291 (1985).
[7]G. P. Yost *et al.*, Phys. Lett. B **204**, 1 (1988).
[8]S. Theberge, A. W. Thomas, and G. A. Miller, Phys. Rev. D **22**, 2838 (1980); **23**, 2106(E) (1981); A. W. Thomas, S. Theberge, and G. A. Miller, *ibid.* **24**, 216 (1981); S. Theberge, G. A. Miller, and A. W. Thomas, Can. J. Phys. **60**, 59 (1982); A. W. Thomas, Adv. Nucl. Phys. **13**, 1 (1984).
[9]E. A. Veit, B. K. Jennings, and A. W. Thomas, Phys. Rev. D **33**, 1859 (1986).
[10]E. A. Veit, A. W. Thomas, and B. K. Jennings, Phys. Rev. D **31**, 2242 (1985).
[11]A. W. Thomas, J. Phys. G **7**, L283 (1981); A. Szymacha and S. Tatur, Z. Phys. C **7**, 311 (1981).
[12]E. A. Veit, B. K. Jennings, A. W. Thomas, and R. C. Barret, Phys. Rev. D **31**, 1033 (1985).
[13]G. F. Chew, Phys. Rev. **94**, 1755 (1954); G. F. Chew and F. E. Low, *ibid.* **101**, 1570 (1956); **101**, 1579 (1956).
[14]A. S. Rinat, Nucl. Phys **A377**, 341 (1982).
[15]B. C. Pearce and I. R. Afnan, Phys. Rev. C **34**, 991 (1986).
[16]E. D. Cooper and B. K. Jennings, Phys. Rev. D **33**, 1509 (1986).
[17]I. R. Afnan and B. C. Pearce, Phys. Rev. C **35**, 737 (1987).
[18]I. R. Afnan and B. Blankleider, Phys. Rev. C **22**, 1638 (1980); B. Blankleider and I. R. Afnan, *ibid.* **24**, 1572 (1981).
[19]B. Blankleider, Ph.D. thesis, Flinders University of South Australia, 1981.
[20]I. R. Afnan and B. Blankleider, Phys. Rev. C **32**, 2006 (1985).
[21]M. G. Fuda, Phys. Rev. C **30**, 666 (1984); **31**, 1365 (1985); **32**, 2024 (1985).
[22]H. Garcilazo and L. Mathelitsch, Phys. Lett. B **205**, 199 (1988).
[23]B. C. Pearce, Phys. Rev. C **36**, 471 (1987).
[24]D. J. Ernst, C. M. Shakin, and R. M. Thaler, Phys. Rev. C **8**, 46 (1973); **8**, 2056 (1973).
[25]I. R. Afnan and A. W. Thomas, Phys. Rev. C **10**, 109 (1974).
[26]B. C. Pearce, Ph.D. thesis, Flinders University of South Australia, 1986.

[27]G. Höhler, F. Kaiser, R. Koch, and E. Pietarinen, *Handbook of Pion-Nucleon Scattering* (Fachinformationszentrum Energie-Physik-Mathematik, Karlsruhe, 1979).
[28]J. A. Johnstone and T.-S. H. Lee, Phys. Rev. C **34**, 243 (1986).
[29]E. Umland, I. Duck, and W. von Witsch, Phys. Rev. D **27**, 2678 (1983).
[30]L. R. Dodd, A. W. Thomas, and R. F. Alvarez-Estrada, Phys. Rev. D **24**, 1961 (1981).